RESEARCH ARTICLE
doi: 10.2306/scienceasia1513-1874.2025.086

ScienceAsia 51 (5): 2025: ID 2025086: **1–6**

Porous ceramics from Saudi mineral materials

N. M. Khalil[a,*], **Yousif Algamal**[a,b]

[a] Chemistry Department,The Applied College–Khulais, Jeddah 21959, University of Jeddah, K.S.A.
[b] Chemistry Department, Faculty of Science & Technology, Omdurman Islamic University, Sudan

[*]Corresponding author, e-mail: nagy2071@yahoo.com

Received 9 May 2024, Accepted 29 Sep 2025
Available online 31 Oct 2025

ABSTRACT: One of the 2030 Vision goals of the Kingdom of Saudi Arabia (KSA) is industrial development through the exploitation of local resources. Local bauxite ore and alumina extracted from aluminum workshop wastes were used to prepare several porous ceramic bodies by adding a constant percentage of fly ash as a pore-forming agent. Correspondence mixes of dense ceramic bodies were prepared without the addition of fly ash for comparison. Studying the sintering (bulk density and apparent porosity), mechanical strength (cold crushing strength), electrical resistivity, and thermal conductivity of the fired ceramic bodies indicated that the porous ceramic bodies prepared from 60 wt% bauxite and 40 wt% alumina with the addition of 10 wt% fly ash exhibits a good combination of sintering (bulk density; 3.70 g/cm^3, apparent porosity 10.11%), mechanical strength (290 kg/cm^2), electrical resistivity (5.00×10^9 ohm.m) and thermal conductivity (0.051 W.m^{-1}.K^{-1}) properties due to its outstanding assemblage of mineral compositions (mullite-cristobalite-anorthite) which enable their use as promised materials in a wide range of traditional and advanced applications.

KEYWORDS: porous ceramics, fly ash, bauxite ore, mineral wastes, mechanical properties

INTRODUCTION

The issue of energy conservation is one of the most important issues on the economic and social levels. Until now, the criterion by which energy conservation in buildings is measured as the development of thermally insulating ceramic materials [1].

The term porous ceramics is applied to ceramic materials with a porosity between 20 and 95% in which two phases can be recognized: solid phase and porous phase. Because of their unique properties involving good mechanical strength and abrasion resistance, high permeability, low-density, and low thermal conductivity as well as good thermal and chemical stability, porous ceramics have attracted the attention of researchers and industrialists in the last two decades [2, 3].

The combination of these properties in porous ceramics enables their utilization in numerous wide-ranging applications, such as filters for dust collectors, thermal insulators, absorbents, bioreactors, hot gas collectors, and car engine components, as well as ceramic membranes. The quality of porous ceramics depends on several factors, some of which are the materials used in their manufacturing, pore size, pore size distribution, particle size, particle size distribution, surface, shape, manufacturing techniques, sintering effect, pore connections, type of binder used, etc.

Chen et al [4] prepared porous ceramics from aluminum borate and studied the effect of the aluminum/boron molar ratio on their properties. The effect of composition on the thermal conductivity of porous ceramics based on calcium hexa-aluminate was studied [5, 6]. Saloma et al [7] prepared porous alumina-spinel ceramics for use in high-temperature applications. Several authors [8, 9] studied the physico-mechanical properties of alumina and magnesium aluminate spinel-based ceramics. Dhara et al [10] and many authors [11–13] succeeded in preparing an outstanding ceramic foam.

Other authors pay attention to mullite-based ceramics as promised materials for electronics and high-temperature applications [14–18]. Han et al [19] investigated the high energy storage performance of $(1-x)Ba_{0.9}Ca_{0.1}TiO_3$-$xBaSn_{0.1}Ti_{0.9}O_3$ ceramics. There are several research works on manufacturing refractory materials from raw minerals and industrial waste [20–23]. Wahsh et al [24] studied the technological properties of porous ceramics based on the forsterite-spinel-zirconia system. Several recent research works have been published that deal with the classification, various techniques and methods used for the preparation of porous ceramics [25–27]. Bin Xia et al [28] studied the performance and mechanical properties of fly ash-based porous ceramics. A recent study by Jaita et al [29] reported improved apatite-forming ability of nano-hydroxyapatite bioceramics when modified with $Bi_{0.50}(Na_{0.80}K_{0.20})_{0.5}TiO_3$.

The world, in general, and the Kingdom of Saudi Arabia, in particular, suffer from air pollution problems due to the emission of hot gases from various mining industries. Therefore, there is a global trend to reduce the emission of gases that cause air pollution problems by promoting clean sectors. Researchers worldwide have explored various ideas, including the development of ceramic filters to reduce these harmful gases. One of the vision goals, in line with trends of the Kingdom of Saudi Arabia, through Vision 2030,

is to maximize the utilization of its natural mineral wealth in the development of industries, to prepare porous ceramics. These ceramics can be used as filters for harmful gases, thereby contributing to environmentally friendly industrial processes. This work thus aims at the exploitation of vast quantities of aluminum scraps wasted from aluminum workshops together with local bauxite ore to manufacture mullite-based porous ceramics.

MATERIALS AND METHODS

Materials

Bauxite mineral, sourced from the eastern region of KSA (Zubiera region), was processed and used as a source of alumina (Al_2O_3). Alumina was extracted from aluminium scrap wastes. Industrial fly ash wasted from the Rabigh electricity plant was used as a pore-forming agent.

Chemical composition of the starting materials

Chemical analyses of the starting materials were detected using the X-ray fluorescence technique (XRF, Bruker, Germany). As given in Table 1, the used bauxite contains considerable contents of Al_2O_3 (77.10%) and relatively lower content of SiO_2 (6.50%) with lower contents of other oxides as impurities. Loss on ignition (LOI) of bauxite determined by firing was 10.68% while in fly ash it reaches 89.01%. The table below indicates the high purity of the alumina used (99.80% Al_2O_3). Considering the chemical compositions of the starting materials, the mineral mullite ($3\,Al_2O_3 \cdot 2\,SiO_2$) with unique thermomechanical properties is expected to be formed after firing [18, 20].

Methods

Ceramic batches preparation

Based on the chemical composition of the starting materials, ten batches were composed of different contents of bauxite and alumina, for five of which 10 wt% of fly ash was added as a pore-forming agent to prepare porous ceramic bodies (this percentage was chosen based on a previous published work [30]), others were designed without fly ash addition to prepare dense ceramic bodies for comparison (Table 2). The mixtures were separately processed through manual mixing, followed by 1 h in an alumina ball mill to ensure homogeneity. The individual batches were well mixed in a ball mill for 2 h and then shaped into cylindrical bodies through uni-axial semi-dry pressing at 150 MPa. The obtained green bodies were dried overnight at 110 °C and then fired at 1500 °C with a firing rate of 10 °C/min and a soaking time of 2 h [31].

Characterization

X-ray diffraction (D8-Advance, Bruker; monochromatic beam with Kα1 Cu, 40 kV, 40 mA) was used to investigate the phase composition of a selected sample of the fired ceramic bodies. The microstructure of the selected sample was depicted with a scanning electron microscope (SEM-JEOL JAX-840A electron microanalyzer, Japan). Bulk density and apparent porosity were determined using the boiling water method according to ASTM C373 [32]. Cold crushing strength (CCS) was measured using a hydraulic pressing machine following ASTM C133 [33]. Thermal conductivity was determined using a modulated temperature differential scanning calorimeter method in accordance with ASTM E1952 [34]. Electrical resistivity was measured at room temperature using a standard two-probe technique [35].

The preparation and testing steps are summarized in the following flowchart.

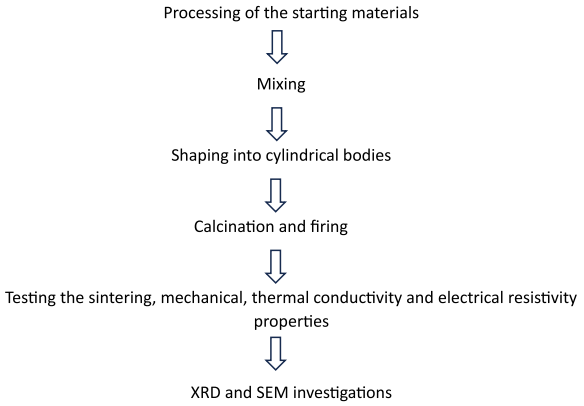

Fig. 1 Flowchart illustrating the preparation and testing steps of ceramic bodies.

RESULTS AND DISCUSSION

Sintering parameters

Fig. 2 shows the bulk density and apparent porosity of the prepared dense and porous ceramics. The result shows a steadily increase in the bulk density values of either dense or porous ceramic bodies corresponded with a decrease in the apparent porosity percentages as we proceed from C1 to C4 (3.41–3.7 g/cm^3, 12.40–10.11%) or from PC1 to PC4 (2.87–3.01 g/cm^3, 18.50–16.02%) beyond which (in C5 or PC5) a noticeable decrease in bulk density (3.4 g/cm^3, 2.85 g/cm^3) corresponded with a marked increase in the apparent porosity (10.96%, 17.12%) was observed. This behavior is related to the decrease in the alumina content and the increase in bauxite content rich in silica that enhances the chance of mullite mineral ($3\,Al_2O_3 \cdot 2\,SiO_2$) formation, which interlock together with cristobalite (SiO_2) and the glassy phases (anorthite; $2\,CaO \cdot Al_2O_3 \cdot SiO_2$) resulting in the matrix of dense and porous ceramics — an increase in density and a decrease in porosity. However, a further increase in bauxite content (C5 or PC5) results in the formation of a relatively higher content of glassy phases that

Table 1 Chemical constitution of the used materials.

Material	Fe_2O_3	MgO	Na_2O	K_2O	SO_3	SiO_2	CaO	Al_2O_3	TiO_2	Cr_2O_3	LOI
Bauxite	1.20	0.80	–	–	–	6.50	0.80	77.10	2.12	0.80	10.68
Fly ash	–	–	0.13	0.07	1.61	6.08	0.40	2.70	–	–	89.01
Alumina	0.05	–	–	–	–	0.08	0.05	99.80	0.02	–	–

Table 2 Green Ceramic Batches.

Sample No.	Batch No.	% wt Bauxite	% wt Alumina (Al_2O_3)	% wt Porous-forming agent (fly ash)
1	C1	30	70	0
2	C2	40	60	0
3	C3	50	50	0
4	C4	60	40	0
5	C5	70	30	0
6	PC1	30	70	10
7	PC2	40	60	10
8	PC3	50	50	10
9	PC4	60	40	10
10	PC5	70	30	10

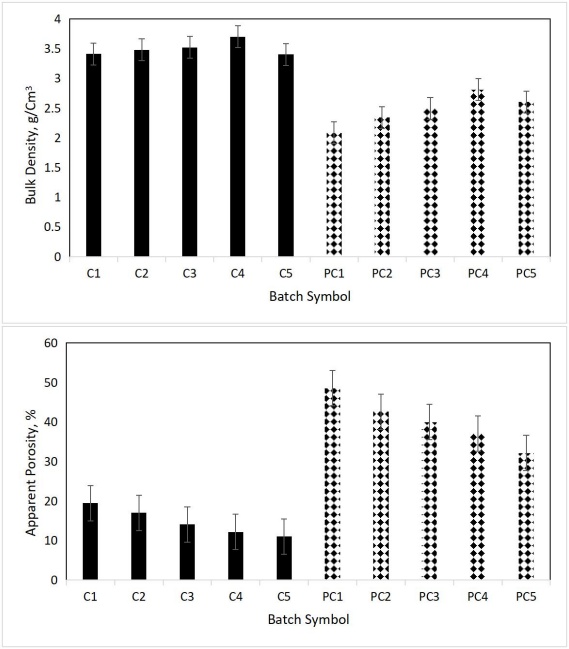

Fig. 2 Bulk density and Apparent porosity of the prepared ceramic bodies.

affect adversely the mullitization process and hence the decrease in density and increase in porosity [36]. Generally, the porous ceramics (PC1–PC5) show relatively lower values of bulk density and a higher percent of apparent porosity compared with the correspondence dense ceramic bodies (C1–C5) due to the presence of 10 wt% fly ash in the green composition of porous

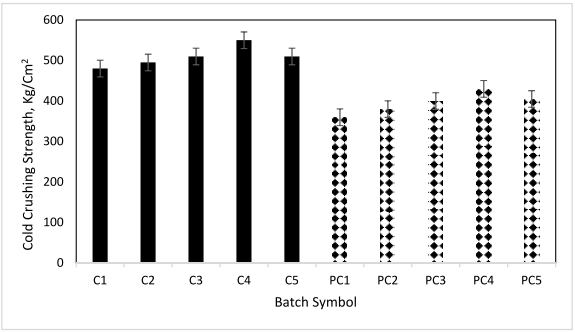

Fig. 3 Cold crushing strength of the prepared ceramic bodies.

ceramic mixes that mostly lost as released as gases on firing (LOI of fly ash is 89.01%, as given in Table 2) leaving a porous matrix [27].

Mechanical properties

Fig. 3 shows the cold crushing strength of the prepared porous ceramics compared with the dense ones. The result shows a gradual increase in the cold crushing strength values of either dense or porous ceramics as the bauxite content increases at the expense of alumina content, reaching their maximum values at the mix C4 in dense or PC4 in porous ceramics containing 60 wt% bauxite and 40 wt% alumina, beyond which (C5 or PC5) a marked decrease in the values or cold crushing is observed. Further increase in the bauxite content to more than 60 wt% results in the formation of relatively higher content of glassy phases as a result of the impurities of bauxite mineral which affect adversely the mullite mineral formation leading to a noticeable decrease in the cold crushing strength values [22, 27]. The figure shows also a relative decrease in the values of cold crushing strength of the porous ceramic mixes compared to their counterparts of dense mixes that is due to the relatively higher porosity and lower density of the porous ceramic mixes. However, they could maintain reasonable cold crushing strength values (170–230 kg/cm^2) as we proceed from PC1 to PC4 compared with C1–C4 (230–290 kg/cm^2) i.e., the porous ceramics could attain 73.91–79.31% of the corresponding dense ceramic bodies' strength due to good assemblage of mineral system (mullite-glassy phases) either in dense or in porous samples.

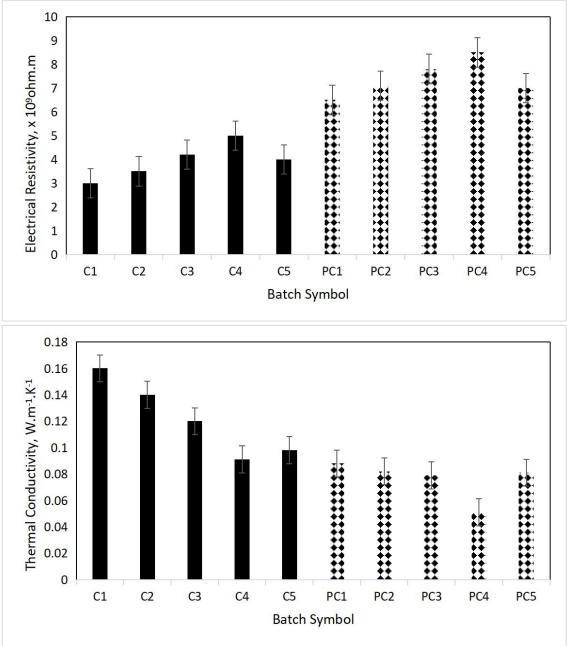

Fig. 4 Electrical resistivity and thermal conductivity of the prepared ceramic bodies.

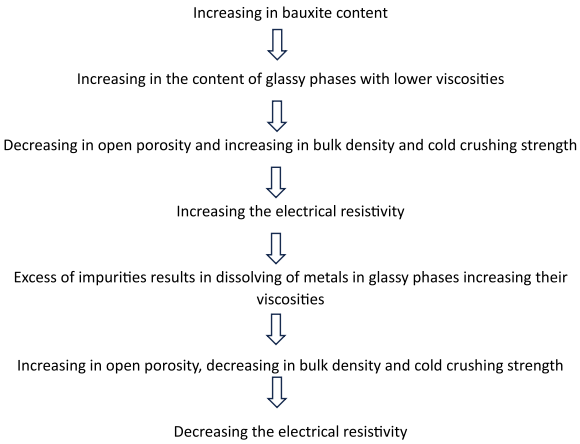

Fig. 5 Schematic diagram for sintering, mechanical and electrical properties behavior for the prepared ceramic bodies.

Electrical resistivity and thermal conductivity

As shown in Fig. 4, the porous ceramics show relatively higher electrical resistivity compared with their correspondence in dense ceramic bodies. The figure shows also an improvement in electrical resistivity of either dense or porous ceramic as we proceed from C1 to C4 (3×10^9–5×10^9 ohm.m) or PC1 to PC4 (6.5×10^9–8.5×10^9 ohm.m) i.e., as the content of bauxite mineral increases in the green mix at the expense of the alumina content reaching its maximum value with C4 (5×10^9 ohm.m) and PC4 (8.5×10^9 ohm.m)

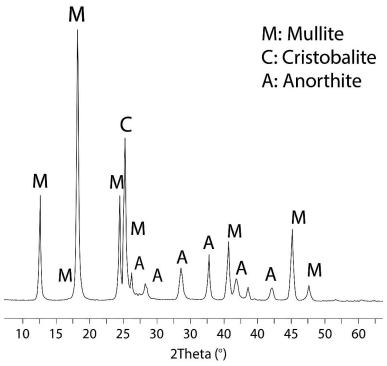

Fig. 6 XRD patterns of PC5 ceramic body.

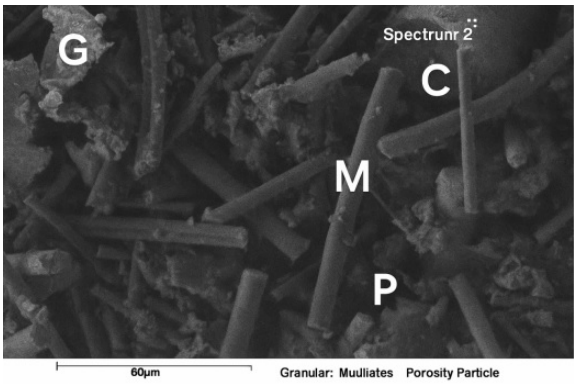

Fig. 7 SEM photomicrograph of PC5 ceramic body (G: Glassy phase; C: Cristobalite, M: Mullite, P: Pores).

but decrease again with C5 (4×10^9 ohm.m) or PC6 (7×10^9 ohm.m).

Fig. 4 also shows the thermal conductivity of the prepared dense and porous ceramic samples. The result shows a gradual decrease in the values of thermal conductivity as we proceed from C1 to C4 (0.016–0.091 $W.m^{-1}.K^{-1}$) and from PC1 to PC4 (0.088–051 $W.m^{-1}.K^{-1}$). Beyond them, i.e., in C5 and PC5, the thermal conductivity is increased (0.098, 0.081 $W.m^{-1}.K^{-1}$). It was found that the PC4 mix shows the lowest value of thermal conductivity (0.051 $W.m^{-1}.K^{-1}$) among the samples investigated. An explanation of this behavior is illustrated in the scheme shown in Fig. 5. The increase in electrical resistivity and the decrease in thermal conductivity as the bauxite content increases in the green mix at the expense of the alumina content, i.e., from C1 to C4 or PC1 to PC4 is correlated with the mullite mineral formation together with cristobalite and the anorthite glassy phases with lower viscosity. This leads to better electrical resistivity, the positive effect is reversed on over-increasing in the content of the glassy phases in which metals dissolve leading to decreasing viscosity of the glassy phases and hence decreasing the electrical

resistivity which is the case in C5 and PC5 [28, 36–38]. Based on the previous evaluations, mix PC4 was chosen as optimum sample and selected for further XRD and SEM investigation. Fig. 6 shows the XRD patterns of PC4 samples in which the lines characterizing mullite predominates, also some lines characterizing cristobalite and anorthite glassy phases could be detected.

Fig. 7 shows the microstructure of PC4 that indicates rod-like crystals characterizing mullite (M) spread in the matrix with the presence of glassy phases (G) and cristobalite (C) with considerable contents of pores among these crystals. The improvement in the physico-mechanical properties of ceramic bodies prepared from mix 4 is correlated with its outstanding assemblage of minerals (mullite-cristobalite-anorthite). The high content of mullite characterized by high mechanical, low electrical conductivity, and low thermal conductivity [35] reflects its advantages on ceramic bodies of mix 4. The presence of some content of low melting cristobalite and anorthite leads to the formation of some liquid phases that fill voids and cavities resulting in an improvement in sintering and hence mechanical properties. The presence of considerable contents of pores among the rod-like mullite, cristobalite, and anorthite crystals shown in the SEM photomicrograph (Fig. 6) is another factor added to the lower electrical conductivity of mullite causing the relatively high electrical resistivity of such sample compared with the published data for porous ceramics prepared using other types of pore forming agents [2, 13, 39, 40]. The superior performance of this composition is attributed to the formation of an optimized mineralogical assemblage comprising mullite, cristobalite, and anorthite, as confirmed by XRD and SEM analyses. Mullite's high mechanical strength and low thermal/electrical conductivity, combined with the glassy phase's densification effect and controlled porosity, result in a well-balanced multifunctional ceramic material. Compared to globally reported porous ceramics, the present materials demonstrate competitive or superior properties, with the added advantages of cost reduction, sustainability, and alignment with national industrial development goals.

CONCLUSION

Porous ceramic bodies could be prepared from 60% local bauxite and 40% alumina using 10 wt% of fly ash as a pore-forming agent. This is an efficient assemblage of minerals (mullite-cristobalite-anorthite) which leads to a good compromise between good sintering, high mechanical, high electrical resistivity, and low thermal conductivity, enabling their use in a wide range of various traditional and advanced applications, e.g., insulating refractories, pottery, porcelain, IR transparent window, car engine component, electronics.

Acknowledgements: This research project is funded by the Deanship of Research and Post-graduate Studies of the University of Jeddah, Saudi Arabia, Grant No. (UJ-21-DR-11).

REFERENCES

1. Zhao-hui Z, Xiang-bo S, Fu-chi W, Sai W, Shu-kui L (2013) Microstructure characteristics and mechanical properties of TiB/Ti-1.5Fe-2.25Mo composites synthesized in situ using SPS process. *Trans Nonferrous Met Soc China* **23**, 2598–2604.
2. Hong-nian C (2013) Microstructure characteristics and mechanical properties of TiB/Ti-1.5Fe-2.25Mo composites synthesized *in situ* using SPS process. *Trans Nonferrous Met Soc China* **23**, 2598–2604.
3. Yang F, Zhao S, Chen G, Li K, Fei Z, Mummery P, Yang Z (2024) High-strength, multifunctional and 3D printable mullite-based porous ceramics with a controllable shell-pore structure. *Adv Powder Mater* **3**, 100153.
4. Chen G, Yang F, Zhao S, Li K, Chen J, Fei Z, Yang Z (2022) Preparation of high-strength porous mullite ceramics and the effect of hollow sphere particle size on microstructure and properties. *Ceram Int* **48**, 19367–19374.
5. Dong Y, Dong X, Li L, Wu J, Yan L, Liu J, Guo A (2021) Lightweight and thermally insulating aluminum borate nanofibrous porous ceramics. *Ceram Int* **47**, 21029–21037.
6. Yuan L, Jin E, Li C, Liu Z, Tian C, Ma B, Yu J (2021) Preparation of calcium hexaluminate porous ceramics by novel pectin based gelcasting freeze-drying method. *Ceram Int* **47**, 9017–9023.
7. Saloma R, Villas Boâs MOC, Pandolfelli VC (2011) Porous alumina-spinel ceramics for high temperature applications. *Ceram Int* **37**, 1393–1399.
8. Salvini VR, Innocentini MDM, Pandolfelli VC (2000) Optimizing permeability, mechanical strength of ceramic foams. *Am Ceram Soc Bull* **79**, 49–63.
9. Ueno S, Akatsu T, Nakajima H (2006) Preparation and properties of porous alumina ceramics with oriented cylindrical pores produced by an extrusion method. *J Eur Ceram Soc* **26**, 957–960.
10. Dhara S, Bhargava P (2003) A simple direct casting route to ceramic foams. *J Am Ceram Soc* **86**, 1645–1650.
11. Tang F, Fudouzi H, Sakka Y (2003) Fabrication of macroporous alumina with tailored porosity. *J Am Ceram Soc* **86**, 2050–2054.
12. Thijs I, Luyten J, Steven M (2003) Producing ceramic foams with hollow spheres. *J Am Ceram Soc* **87**, 170–172.
13. Garrn I, Reetz C, Brandes N, Kroh LW, Shubert H (2004) Clot-forming: the use of proteins as binders for producing ceramic foams. *J Eur Ceram Soc* **24**, 579–587.
14. Kritikaki A, Tsetsekou A (2009) Fabrication of porous alumina ceramics from powder mixtures with sol–gel derived nanometer alumina: Effect of mixing method. *J Eur Ceram Soc* **29**, 1603–1611.
15. Tavangarian F, Emadi R (2011) Synthesis and characterization of spinel–forsterite nanocomposites. *Ceram Int* **3**, 2543–2548.
16. Dong Y, Lin B, Xie K, Wang S, Ding H, Fang D, Liu X, Meng G (2009) Cost-effective macro-porous mullite-corundum ceramic membrane supports derived from the industrial grade powder. *J Alloys Compd* **477**, 350–356.

17. Akpinar S, Altun A, Onel K (2010) Effects of SiC addition on the structure and properties of reticulated porous mullite ceramics. *J Eur Ceram Soc* **30**, 2727–2734.
18. Miao X (1999) Porous mullite ceramics from natural topaz. *Mater Lett* **38**, 167–172.
19. Han S, Cui L, Li Z, Luan K (2024) High energy storage performance of $(1-x)Ba_{0.9}Ca_{0.1}TiO_3$-$xBaSn_{0.1}Ti_{0.9}O_3$ bulk ceramics. *ScienceAsia* **50**, ID 2024092.
20. Ebadzadeh T (2005) Porous mullite–ZrO_2 composites from reaction sintering of zircon and aluminum. *Ceram Int* **31**, 1091–1095.
21. Khalil NM, Yousif A, Qyied S (2018) Exploitation of petroleum waste sludge with local bauxite raw material for producing high-quality refractory ceramics. *Ceram Int* **44**, 18516–18527.
22. Khalil NM, Yousif A, Saleem MAQ, Kamal AA, Wahsh MMS (2019) Improved refractory aluminosilicate bricks through nano zirconia additions. *Int J Thin Film Sci Technol* **8**, 131–137.
23. Khalil NM, Yousif A (2020) Recycling of ceramic wastes for the production of high performance mullite refractories. *Silicon* **12**, 1557–1565.
24. Wahsh MMS, Khattab RM, Khalil NM, Gouraudq F, Huger M, Chotard T (2014) Fabrication and technological properties of nanoporous spinel/forsterite/zirconia ceramic composites. *Mater Des* **53**, 561–567.
25. Ohji T, Fukushima M (2012) Macro-porous ceramics: processing and properties. *Int Mater Rev* **57**, 115–131.
26. Gaudillere C, Serra JM (2016) Freeze-casting: fabrication of highly porous and hierarchical ceramic supports for energy applications. *Bol Soc Esp Ceram Vidrio* **55**, 45–54.
27. Eom JH, Kim YW, Raju S (2013) Processing and properties of macroporous silicon carbide ceramics: A review. *J Asian Ceram Soc* **1**, 220–242.
28. Bin X, Zhipeng W, Lizheng G, Mei Z, Min G (2022) Porous mullite ceramics with enhanced compressive strength from fly ash-based ceramic microspheres: Facile synthesis, structure, and performance. *Ceram Int* **34**, 10472–10479.
29. Jaita P, Wannasut P, Khamman O, Watcharapasorn A, Jarupoom P (2025) Enhanced mechanical, electrical, and *in vitro* apatite-forming ability of the nano-hydroxyapatite bioceramics via $Bi_{0.50}(Na_{0.80}K_{0.20})_{0.5}TiO_3$ addition. *ScienceAsia* **51S**, ID 2025s017.
30. Rugele K, Lehmhus D, Hussainova I, Peculevica J, Lisnanskis M, Shishkin A (2017) Effect of fly-ash cenospheres on properties of clay-ceramic syntactic foams. *Materials* **10**, 828.
31. Khalil MN, Wahsh MMS, Gaber A (2016) The effect of albite additions on the sintering, phase compositions and microstructure of vitreous ceramic tile. *J Ceram Process Res* **17**, 478–484.
32. ASTM (2018) *Standard Test Method for Water Absorption, Bulk Density, Apparent Porosity, and Apparent Specific Gravity of Fired Whiteware Products*, American Society for Testing and Materials, West Conshohocken, PA, USA, 2018.
33. ASTM (1997) *Standard Test Methods for Cold Crushing Strength and Modulus of Rupture of Refractories*, American Society for Testing and Materials, West Conshohocken, PA, USA, 1997.
34. ASTM (2017) *Standard Test Method for Thermal Conductivity and Thermal Diffusivity by Modulated Temperature Differential Scanning Calorimetry*, *American Society for Testing and Materials*, West Conshohocken, PA, USA, 2017.
35. Yadunath S (2013) Electrical resistivity measurements: A review. *Int J Mod Phys Conf Ser* **22**, 745–756.
36. Yang Z, Yang F, Zhao S, Li K, Chen J, Fei Z, Chen G (2021) *In-situ* growth of mullite whiskers and their effect on the microstructure and properties of porous mullite ceramics with an open/closed pore structure. *J Eur Ceram Soc* **41**, 299–308.
37. Coutinho NC, Paes HR, Holanda JNF (2022) Effect of firewood ash waste on the densification behavior of electrical siliceous porcelain formulations. *Silicon* **14**, 10591–10601.
38. Roy R, Das D, Rout PK (2022) A review of advanced mullite ceramics. *Eng Sci* **18**, 20–30.
39. Lima LKS, Silva RR, Menezes LR, Santana LNL, Lira HL (2022) Microstructural characteristics, properties, synthesis and applications of mullite: A review. *Ceramica* **68**, 126–142.
40. Liao X, Chen L, Xie Y, Tan J, Luo X, Li H (2023) Microstructural characteristics, properties, synthesis and applications of mullite: A review. *J Phys Chem Solids* **180**, 111465.